biophysica

MDPI

Article

Intermolecular FRET Pairs as An Approach to Visualize Specific Enzyme Activity in Model Biomembranes and Living Cells

Igor D. Zlotnikov [1], Alexander A. Ezhov [2] and Elena V. Kudryashova [1,*]

[1] Faculty of Chemistry, Lomonosov Moscow State University, Leninskie Gory, 1/3, 119991 Moscow, Russia; zlotnikovid@my.msu.ru
[2] Faculty of Physics, Lomonosov Moscow State University, Leninskie Gory, 1/2, 119991 Moscow, Russia
* Correspondence: helenakoudriachova@yandex.ru

Abstract: Herein, we propose an analytical approach based on intermolecular fluorescent resonant energy transfer (FRET) pairs for the visualization of specific enzyme activity in model biomembranes and in living cells. Cell visualizations with fluorescent confocal laser microscopy usually rely on fluorescent probes, such as Fluorescein isothiocyanate (FITC), Alexa488, Tetramethylrhodamine isothiocyanate (TRITC) and many others. However, for more specific tasks, such as the detection of certain enzymatic activity inside the living cell, the toolbox is quite limited. In the case of enzyme-hydrolases for example, the choice is limited to organic molecules comprising a fluorescent dye (typically, 4-methylumbelliferone (MUmb) or 7-amino-4-methylcoumarin (AMC) derivatives) and a fluorescence quencher, bound via an enzyme-sensitive linker—so that when the linker is degraded, the fluorescent signal increases. Unfortunately, both MUmb and AMC are quenched and have a relatively low quantum yield in cells, and their excitation and emission ranges overlap with that of intracellular fluorophores, often producing a strong background noise. R6G, on the other hand, has excellent quantum yield apart from intracellular fluorophores, but there are no efficient quenchers that could be chemically linked to R6G. Herein, we show that R6G is able to form intermolecular FRET pairs with MUmb or AMC, with the latter serving as fluorescence donors. This yields a combination of R6G's excellent fluorescence properties with a possibility to use an enzyme-sensitive linker in MUTMAC or AMC derivatives. This phenomenon was initially discovered in a model system, reversed micelles, where the donor, the acceptor, and the enzyme are forced to be in close proximity to each other, so that proximity could serve as an explanation for the intermolecular FRET effect. Surprisingly enough, the phenomenon has been reproduced in living cells. Moreover, we were able to create working intermolecular donor–acceptor FRET pairs for several different enzymes, including chymotrypsin, phosphatase, and asparaginase. This appears counterintuitive, as besides the overlap of the emission spectra of the donor and the absorption spectra of the acceptor, there are other criteria for the FRET effect, including the convergence of two fluorophores at a distance of about 1–10 nm, and the orientation of their dipoles at a certain angle, which is difficult to imagine in a bulk system like a living cell. We hypothesize that FRET-enabling donor–acceptor interaction may be taking place at the inner surface of the lipid bilayer, to which both donor and acceptor molecules would likely have an affinity. This hypothesis would require a more detailed investigation. Therefore, we have shown that the method suggested has good potential in the visualization of enzyme functioning inside living cells, which is often a challenging task. Shifting of the fluorescence signal to the long-wavelength region would increase the signal selectivity, making it easily distinguishable from autofluorescence.

Keywords: FRET probes; marker; rhodamine 6G; reverse micelle; intracellular enzyme activity

Citation: Zlotnikov, I.D.; Ezhov, A.A.; Kudryashova, E.V. Intermolecular FRET Pairs as An Approach to Visualize Specific Enzyme Activity in Model Biomembranes and Living Cells. *Biophysica* **2024**, *4*, 340–356. https://doi.org/10.3390/biophysica4030024

Academic Editor: Giuseppe Maulucci

Received: 25 May 2024
Revised: 27 June 2024
Accepted: 28 June 2024
Published: 1 July 2024

1. Introduction

This paper is devoted to developing an analytical approach based on intermolecular fluorescent resonant energy transfer (FRET) pairs for the visualization of specific enzyme activity in model biomembranes and in living cells. There are a number of advantages in

determining the enzymatic activity using the FRET technique. Firstly, the emission maximum is shifted to the long-wavelength region, and a system with a higher quantum yield is obtained, which opens up the possibility of applying this approach to the visualization of processes in cells using confocal laser scanning microcopy (CLSM) [1–4]. Secondly, the FRET technique can reduce fluorescence quenching, particularly in model biomembrane systems such as liposomes and reverse micelles.

In the last decade, the use of FRET as a technique for measuring biochemical parameters has been actively explored [1,5–8]. This tool has proven to be effective due to its sensitivity and specificity. The FRET effect depends on the specific arrangement of molecules in a system, making it a valuable tool for studying biological processes. Changes in the FRET signal can be monitored in real time, providing information about the system's state, for example, its cellular processes. FRET has also been used to create powerful sensors for biological research and medical applications, such as sensors for detecting specific molecules or detecting changes in cell behavior [6,9–11].

The FRET signal is observed when three conditions coincide [3,12,13]: (1) overlapping of the emission spectra of the fluorescence of the donor and the absorption of the acceptor, (2) convergence of the fluorophores at a distance of about 1–10 nm, and (3) orientation of the dipoles at an angle significantly different from the straight one—these are quite specific conditions.

Fluorescent probes, in conjunction with optical systems, form the basis for FRET technology, but also for the complementary approaches such as fluorescence lifetime imaging microscopy (FLIM) and fluorescence recovery after photobleaching (FRAP) [14–16]. The high-resolution FLIM method allows for the recording of delayed fluorescence attenuation following pulsed laser irradiation in a wide field of view. This allows for the acquisition of a fluorescent image across a large area, eliminating inaccuracies during the image acquisition process [16]. FLIM is used to assess the metabolic status of cells based on NAD^+/NADH levels, which are key indicators of cellular energy metabolism [17]. $NAD(P)^+$ is central to the processes of biosynthetic activity and antioxidant defense. FLIM enables us to quantitatively differentiate between the two coenzymes NADH and NAD [17]. Furthermore, FLIM microscopy has made it possible to determine the enzymatic activity of red proteins in living HT-1080 cells [18]. FRAP is used to investigate the molecular dynamics within and on the surfaces of cells [14,19,20]. Fluorophores are used to detect changes in the cell's microenvironment. The combination of the described microscopy techniques allows one to obtain information about molecular interactions with high resolution.

Reversed micelles represent a relevant model of biological membrane structures, as evidenced by the incorporation of non-bilayer structures between the monolayers in a bilayer membrane. With the involvement of lipid particles and associated structures, important cellular processes such as membrane fusion, compartmentalization, exocytosis, and lipid transport across membranes via the flip-flop mechanism, as well as transmembrane ion transport, can occur [21–23]. Certain proteins, such as cytochrome C, are capable of inducing the formation of inverted micelles within a bilayer membrane by inserting themselves into the interior cavity of these micelles [22]. In this regard, the application of the FRET technique to micellar enzymological experiments will allow us to look, with a different focus, at a picture of the functioning of enzymes in model membrane systems. Reverse micelles spontaneously form in a system containing a surfactant, water, and a nonpolar organic solvent. The size of the micelle cavity, where the protein molecules are located, is regulated by changing the hydration degree of the surfactant $W_0 = [H_2O]/[AOT]$ [24]. For reverse AOT micelles, there is a direct correlation between the degree of water content (W_0) and the size of micelles [21–23,25–27]. The catalytic activity of enzymes in micelles usually show a bell-shaped dependence of the catalytic activity on the W_0, with an optimum at conditions where the enzyme size corresponds to the size of the inner cavity of the micelle.

In this work, we used rhodamine 6G (R6G)-based FRET probes [28–32] as a fluorophore acceptor to study the activity of enzymes of different class (chymotrypsin, asparaginase, phosphatase) in a reversed micelles system, as a cell membrane model in which fluorophore

molecules are close to each other due to the small volume of the aqueous phase in comparison with an aqueous solution, and further in living cells. Methylumbelliferone (MUmb) and coumarin (AMC) derivatives were used as enzymatic substrates. The enzyme catalyzes the reaction with the release of fluorescent products—donors in the FRET-pairs with rhodamine 5G. These were converted into products by the enzyme, and as a result, the FRET-based marker R6G was detected. This phenomenon was initially discovered in a model system, reversed micelles, where the donor, the acceptor, and the enzyme are forced to be in close proximity to each other, so that proximity could serve as an explanation for the intermolecular FRET effect. Surprisingly enough, the phenomenon has been reproduced in living cells. Moreover, we were able to create working intermolecular donor–acceptor FRET pairs for several different enzymes, including chymotrypsin, phosphatase, and asparaginase.

Although the determination of catalytic activity using the FRET effect is known, here we suggest a new method of enzyme activity measurement via FRET. Normally, scientists use the FRET substrate in a different way: the FRET substrate is a covalent conjugate, and as a result of the enzymatic reaction, the hydrolysis of the FRET substrate (conjugate) leads to the separation of the fluorophore pair, and FRET is no longer observed. The activity is determined by the decrease in the fluorescence (FRET) signal.

Herein, we propose a completely different analytical approach based on intermolecular FRET pairs for the visualization of specific enzyme activity in model biomembranes, such as AOT reverse micelles, and in living cells, where the compartmentalization and concentration of individual fluorophores occurs. Through this process, the selectivity of the FRET signal in relation to the entire solution can be attained. This approach can be applied to visualize the enzyme functioning in living cells in the condition of their localization in specific cellular structures with, for example, the CLSM technique, where fluorescent probes in the visible area are required with high resolution and signal selectivity (to exclude the autofluorescence). The advantages of the approach include the possibility of choosing suitable FRET pairs; fluorophores being added independently; the possibility of incorporating one of the fluorophores into the system beforehand; and the possibility of detecting several consistent enzymatic biochemical reactions—all of which are useful for research into biochemical pathways in cells. We believe that the method suggested has good potential in the visualization of enzyme functioning inside living cells, which is often a challenging task.

2. Materials and Method

2.1. Reagents

Surfactant AOT (Aerosol OT, sodium bis(2-ethylhexyl) sulfosuccinate) and the fluorophores rhodamine 6G (R6G), 4-methylumbelliferyl p-trimethylammoniocinnamate chloride (MUTMAC), 4-methylumbelliferyl phosphate (MUmb-phosphate), 4-methylumbellifer one (MUmb), L-aspartic acid β-(7-amido-4-methylcoumarin) (Asp-AMC), and 7-amino-4-methylcoumarin (AMC) were purchased from Sigma-Aldrich (St Louis, MI, USA).

Enzymes: α-chymotripsin from bovine pancreas (EC 3.4.21.1, $\geq$40 units/mg protein), acid phosphatase (EC 3.1.3.2), and alkaline phosphatase (EC 3.1.3.1) were purchased from Sigma-Aldrich (St. Louis, MI, USA). Recombinant L-asparaginase from *Erwinia carotovora* (EwA) used in this work was isolated following expression in constructed stain *E. coli* BL21(DE3)/pACYC_LANS (KM). The activity of asparaginase was checked using the method of circular dichroism spectroscopy on a J-815 CD spectrometer (Jasco, Tokyo, Japan), IR spectrometers MICRAN-3 (Simex, Novosibirsk, Russia) and Bruker Tensor 27 IR Fourier spectrometer (Bruker, Ettlingen, Germany) equipped.

2.2. FRET Probes for Determining the Catalytic Activity of Enzymes

2.2.1. FRET Probes

The FRET pairs consisted of a donor (enzyme substrate and catalytic reaction product) and an acceptor (R6G). The final concentration of fluorophores was 1 μg/mL. Fluorophore

emission and excitation spectra were recorded for each separately and for a donor+acceptor mixture in a buffer solution (PBS 0.01M, pH 7.4).

The excitation and emission spectra of fluorescence were recorded on a Varian Cary Eclipse fluorescence spectrometer (Agilent Technologies, Santa Clara, CA, USA).

FRET efficiency **E** was calculated as [13]

$$\mathbf{E} = 1 - F_{DA}/F_D, \quad (1)$$

where F_{DA} and F_D are the intensities of donor fluorescence in the presence and absence of the acceptor, respectively; and F_{AD} and F_A are the intensities of acceptor fluorescence in the presence and absence of the donor, respectively. On the other hand, $E = 1/(1 + (r/R_0)^6)$, where R_0 is the Förster radius, being the distance at which 50% of the excitation energy is transferred from the donor to the acceptor, which is about 5–6 nm in the studied systems.

Therefore, the distance between the fluorophores [13]

$$\mathbf{r} = R_0 \times (1/(F_D/F_{DA} - 1))^{1/6}. \quad (2)$$

R_0 was calculated using Equation (3):

$$R_0 = \sqrt[6]{\left(\frac{0.0247 \times \kappa^2 \times \Phi_D \times J(\lambda)}{\pi^5 \times N_A \times n^4}\right)}, \quad (3)$$

where κ^2 is the orientation coefficient, which may be assumed to be 2/3 in the case of isotropic and randomly oriented donor and acceptor molecules. Φ_D is the fluorescence quantum yield of the donor; $N_A = 6.02 \times 10^{23}$ mol^{-1}; n is the refractive index of the dispersion medium; and J(λ) represents the integral of the spectral overlap. This was calculated using the following equation:

$$J(\lambda) = \frac{\int F_D(\lambda) \times \varepsilon_A(\lambda) \times \lambda^4 d\lambda}{\int F_D(\lambda) d\lambda}, \quad (4)$$

where $F_D(\lambda)$ is the intensity of donor fluorescence, and $\varepsilon_A(\lambda)$ is the molar absorption coefficient of the acceptor.

2.2.2. Fluorometric Determination of Enzyme Activity

The catalytic activity of enzymes was determined fluorometrically: (1) in a buffer solution; (2) in a reversed micellar system; and (3) in living cells. The reaction rate was measured by the accumulation of the fluorescent reaction product and R6G FRET agent: specific parameters are indicated in the captions to the tables and figures. Atomic force microscopy (AFM microscope NTEGRA II, NT-MDT Spectrum Instruments, Moscow, Russia) was used to control the micelles foramtion.

To make a solution of reversed micelles with a given hydration degree (W_0), a certain amount of PBS buffer solution (V_{aq}) was added to 1 mL of micellar solution (V_{mic}) based on the equation V_{aq} (μL) = 18 × C_{AOT} × W_0, where C_{AOT} is the concentration of AOT equal to 0.1 M. The resulting mixture was vigorously shaken until a homogeneous optically transparent solution was formed.

The equations used were as follows [24]:

$$W_0 = C_{aq}/C_{AOT} \quad (5)$$

$$R_{enzyme}\ (Å) = R_{micelle}\ (Å) = 1.5 \times W_0 + 4 \quad (6)$$

where R is the hydrodynamic radii of the enzyme and micelle.

To determine the intracellular activity of L-asparaginase, an enzyme sample (0.5 mg/mL) was incubated with HEK293T cells for 1–4 h at 37 °C, then the cells were thoroughly washed of unabsorbed protein. Then, 5% agarose gel containing 1 mg/mL of MUTMAC substrate

and 1 μM FRET-agent R6G was prepared. Then, 100 μL of fluorescent gel was added to a suspension of 100 μL of HEK293T cells in a 96-well plate and intensively mixed. The gel solidified for several minutes. The samples were then incubated for 4 h at 37 °C for the enzymatic reaction to take place. Cells were visualized using an Olympus FluoView FV1000 confocal microscope (Olympus, Tokyo, Japan), which was equipped with both a spectral version scan unit with emission detectors and a transmitted light detector. The product was developed by the fluorescence of the FRET agent R6G: $\lambda_{exci,max}$ = 515 nm, λ_{emi} = 540–600 nm. The scan area was 80 × 80 μm^2. Olympus FV10 ASW 1.7 software was used for the acquisition of the images.

2.3. HEK293T Cells Cultivation

The embryonic kidney human epithelium HEK293T cell line was obtained from the Lomonosov Moscow State University Depository of Live Systems Collection (Moscow, Russia). Cells were grown in RPMI-1640 medium (Gibco, Thermo Fisher Scientific Inc., Waltham, MA, USA) supplemented with 5% fetal bovine serum (Capricorn Scientific, Ebsdorfergrund, Germany) and 1% Na-pyruvate (Paneco, Moscow, Russia) at 5% CO_2/95% air in a humidified atmosphere at 37 °C.

2.4. Fluorescence Microscopy and Confocal Laser Scanning Microscopy (CLSM) of Cells

Fluorescence images were obtained using a IX81 motorized inverted microscope (Olympus, Tokyo, Japan). A short-arc xenon lamp with a power of 75 W was used as a light source for the fluorescence excitation, and a halogen lamp was used as a light source for transmitted light imaging. Images were acquired using the UPlanSApo 20× NA 0.75 objective lens and U-MWU2 fluorescent filter cube and recorded using the XM10-cooled CCD monochrome camera (all from Olympus, Tokyo, Japan). Cell Sens imaging software (v.3.2, Olympus, Tokyo, Japan) was used for microscope and camera control The use of a fluorescence microscope instead of a confocal laser scanning microscope was due to the fact that ultraviolet light was required to excite fluorescence.

Fluorescence 3D images (Z-stacks) were obtained by the FluoView FV1000 confocal laser scanning microscope (CLSM) (Olympus, Tokyo, Japan) equipped with both spectral version scan unit with emission detectors and transmitted light detector. CLSM is based on the IX81motorized inverted microscope (Olympus, Tokyo, Japan). Emission fluorescence was excited by 515 nm laser light and detected at the wavelength band 530–580 nm. Using the UPlanSApo 20 × NA 0.75 objective lens (Olympus, Tokyo, Japan) provided an axial resolution of no worse than 2 microns at a wavelength of 580 nm. This value was sufficient to show the presence of a fluorophore inside the cells and not just on their surface. FV10 ASW software (v.1.7, Olympus, Tokyo, Japan) was used for acquisition of the images. Obtained images were treated by ImageJ software (v.1.53e, National Institutes of Health, Bethesda, ML, USA).

3. Results and Discussion

3.1. FRET Probes Spectral Properties

To study the enzymatic activity, we used the MUmb-based fluorescent substrates MUTMAC (substrate for protease, α-chymotrypsin), MUmb-phosphate (substrate of phosphatase), and Asp-AMC (substrate of L-asparaginase). The products of these biocatalytic reactions—MUmb, MUmb, and AMC, respectively—have an emission coefficient 1–2 orders of magnitude higher than the substrates (Figure 1). The product served as a fluorescence donor for R6G. In the normalized form (Figure 1), there is obviously a more effective overlap of the fluorescent spectra of the donor and acceptor in the case of products compared to substrates, which further enhances the signal-to-background ratio.

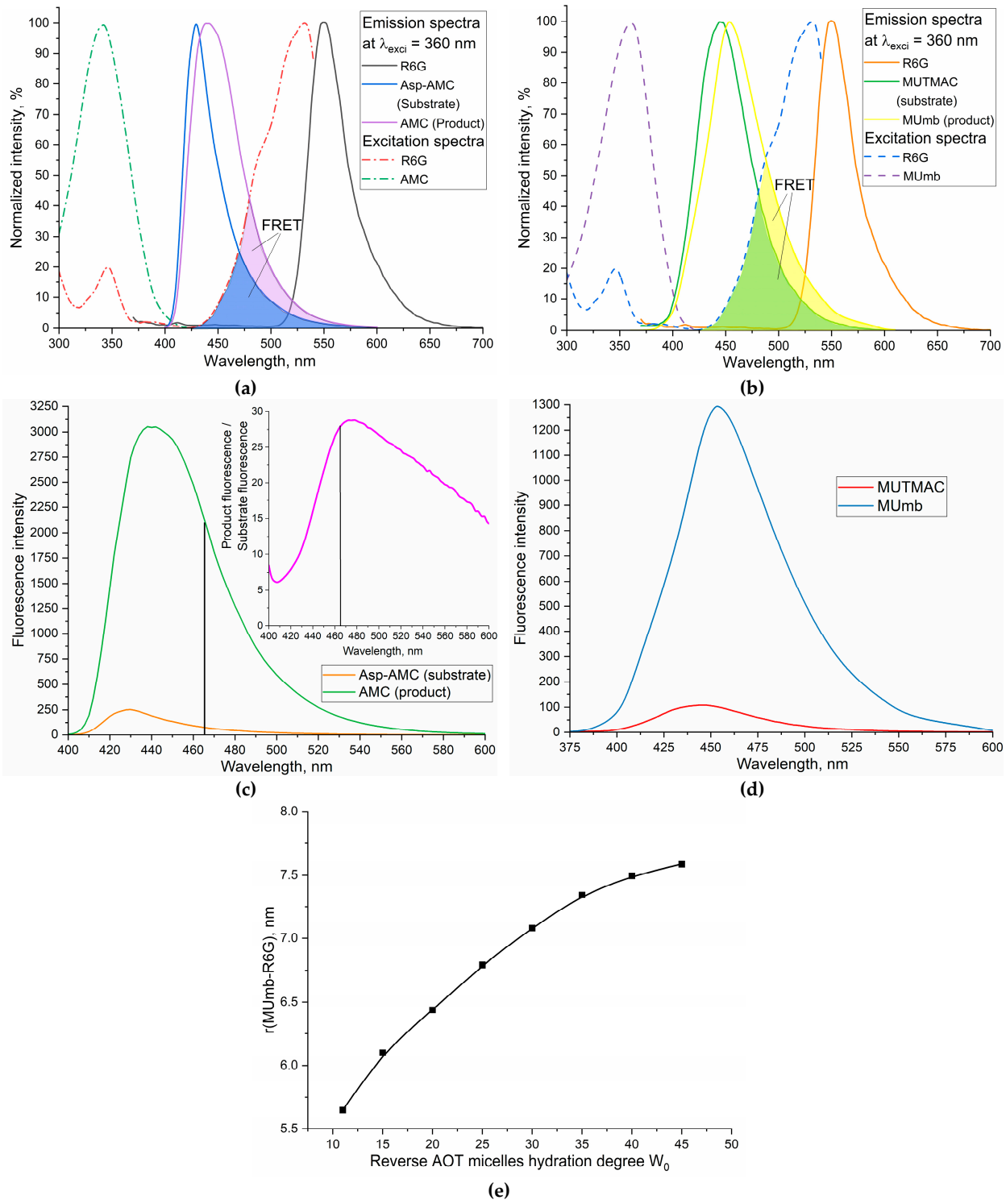

Figure 1. (**a**) Normalized fluorescence spectra of R6G, Asp-AMC, and AMC (1 μM) in PBS buffer solution (0.01M, pH 7.4). (**b**) Normalized fluorescence spectra of R6G, MUTMAC, and MUmb (1 μM) in PBS buffer solution (0.01M, pH 7.4). The maximum excitation wavelength is 360 nm. The emission wavelength is 550 nm for R6G and 440–460 nm for AMC and MUmb derivatives. T = 37 °C. (**c**) Fluorescence emission spectra of Asp-AMC (1 μM) in comparison with AMC (1 μM) in PBS buffer solution (0.01M, pH 7.4), $\lambda_{exci,max}$ = 360 nm. (**d**) Fluorescence emission spectra of MUTMAC (0.25 μM) in comparison with MUmb (1 μM) in PBS buffer solution (0.01 M, pH 7.4), λ_{exci} = 360 nm. T = 37 °C. (**e**) The distance between the fluorophores of the MUmb-R6G FRET pair, depending on the composition of the AOT/octane micellar system.

3.2. Monitoring the Enzyme Catalytic Activity in Buffer Solution vs. Reversed Micellar Systems Using FRET Probes

3.2.1. Theoretical Comparison of Expected FRET Effects in A Buffer and in A System of Reverse Micelles

Previously, we demonstrated that the FRET effect is not as pronounced in aqueous solutions, whereas in micellar systems, this effect is significantly stronger [33]. FRET probes are further applied to study the enzymatic activity in membrane-like systems such as reverse micelles. While in classical surfactant micelles, enzymes tend to denature, the use of reversed micelles makes it possible to solubilize enzymes while maintaining or even enhancing their catalytic activity [24,25,34,35].

Reverse micelles spontaneously form in a tertiary system containing surfactant, water, and non-polar organic solvent. The size of the inner cavity of micelles where protein molecules and other hydrophilic molecules can be entrapped can be strictly controlled by varying the hydration degree ($W_0 = [H_2O]/[AOT]$), which represents the molar ratio of water to surfactant. It has been found that enzymes in reverse micelles normally show a bell-shaped dependence of the catalytic activity on the degree of surfactant hydration, with an optimum at conditions where the enzyme size corresponds to the size of the inner cavity of the micelle [35–38]. With the position of the activity optimum (W_0), one can calculate the inner radius of the micelles, $r_{micelle}$, which can be used to deduce the enzyme maximal radius according to an empirical equation, $r_{micelle}$ (Å) = 1.5 × W_0 + 4. Oligomeric enzymes show activity profiles with several optima, where each of these optima reflects different oligomeric forms of the enzyme. Therefore, reverse micelles can be considered as a "nanoreactor" of molecular size, where one can obtain the desired supramolecular form of the protein or its complexes by controlling of the micellar inner cavity size. The method therefore provides the modulation of enzyme activity and oligomeric composition, as has been demonstrated for a number of enzymes of different classes [24,25,34,35].

This approach offers a perspective to study the details of membrane enzymes functioning and to determine the influence of the membrane lipid compositions on catalytic activity. For example, the reverse AOT micelles are relevant models of mitochondrial membranes. It is known that the mitochondrial membranes contain non-bilayer lipid structures consisting of associates of lipid molecules arranged as reverse micelles incorporated between monolayers of the bilayer membrane. Water–AOT–isooctane is one of the most intensively studied reverse micellar systems for membrane-protein research [22,23,27]. Additionally, reversed AOT-octane micelles are often used to study enzymatic activity to investigate catalytic processes in non-aqueous media and to synthesize or analyze hydrophobic substances. However, in such complex systems, due to high background level, low fluorophore quantum yield, and an unsuitable observation wavelength that interferes with other components of the system, special conditions are required for selective product detection, such as high sensitivity and signal selectivity. This can be achieved with the FRET approach developed here. With this in mind, we applied the FRET approach to study the enzyme activity in reverse micelles.

3.2.2. Objects of Research

Here, we consider α-chymotrypsin, acid and alkaline phosphatase, and L-asparaginase as model membranotropic as well as membrane-independent enzymes catalyzing MUmb or AMC derivatives with the release of MUmb/AMC fluorophores.

FRET is observed in aqueous solutions of MUmb-derivative and R6G, but the FRET effect is rather weak, since the donor and acceptor molecules separate from each other in the volume of the solution [33]. A different situation is observed for reverse micellar system, where the enzyme and the reaction components are located in a limited volume of the aqueous phase of the inner cavity of the micelles.

The fluorescent substrate based on MUmb derivatives is convenient for a number of enzymes. During their enzymatic hydrolysis, the fluorescent product MUmb is released. This effect can be visualized and amplified by FRET: the enzymatic reaction can be moni-

tored by ascending fluorescence of R6G-marker (acceptor) at the 550 nm wavelength. The product release (MUmb) was used as a control parameter, which is reflected in an increase in fluorescence at 450 nm. In reversed micelles, FRET is expected to be more pronounced, due to the concentration of the enzyme and the reaction components in the aqueous phase of the micellar system: MUmb or AMC will be closer to the acceptor R6G, the distance **R** between the fluorophores decreases, and the effectivity of the FRET (**E**) is greater—$E = 1/(1 + (R/R_0)^6)$, where R_0—the Förster radius is the distance at which 50% of the excitation energy is transferred from the donor to the acceptor, which is about 5–6 nm in the studied systems.

3.2.3. FRET Enhancing due to α-Chymotrypsin Activity in AOT-Isooctane Reverse Micelles

The enzymatic activity of α-chymotrypsin in systems of reversed AOT micelles was studied by two parameters: (1) by increasing the fluorescence intensity of the primary product methylumbelliferone, which leads to an intense increase in fluorescence at 450 nm due to a significantly higher emission (quantum yield) of the product and a long-wave shift of the maximum fluorescence emission; and (2) by increasing the fluorescence of R6G (at 550 nm), due to the FRET with MUmb (Figure 2a). Therefore, in addition to monitoring the increase in the fluorescence of R6G, it is possible to monitor the direct response of the release of a fluorescent product (MUmb), as a control. Additionally, the FRET effect can be useful to follow the enzymatic reaction at a specific wavelength interval (for example, 550–600 nm with optical fluorescence microscopy). In addition, there should be no autofluorescent background signal from other cellular components or non-targeted aromatic molecules, as they do not contribute to the overall fluorescent response.

In AOT-octane reversed micelles, an optimum activity (determined by the enzyme molecule size) for α-chymotrypsin is observed at the hydration degree of $W_0 = 11$ (Figure 2b), which is the size of the inner cavity of the micelles corresponding to the geometric size of the enzyme monomer [25]. α-Chymotrypsin catalyzes the hydrolysis reaction of MUTMAC to MUmb (Figure 2a) in the reversed micelles. It turned out that the enzymatic activity at a wavelength of 450 nm (assigned to MUmb) was characterized by low sensitivity compared to the aqueous solution, since the fluorescence of the product is quenched in the micellar system (by more than 45%).

When the FRET effect is realized by including the fluorophore acceptor R6G in the reversed micelles, the sensitivity of the signal increases sharply due to an order-of-magnitude-higher molar emission coefficient of R6G compared to MUmb. Figure 2c shows the sensitivity indexes (the rate of the MUTMAC hydrolysis reaction in the presence of FRET-agent R6G/in the absence of R6G) for determining the rate of MUTMAC hydrolysis reaction in the presence of FRET-agent R6G vs. in the absence of R6G. In the buffer solution and in the system of reversed micelles, the dependence of the sensitivity index on the R6G concentration has a maximum at $C_{R6G} = 5$ and 10 μM, respectively. This is equivalent to MUTMAC:R6G ratios of 40 and 20 (mol/mol), respectively. In the buffer solution, the sensitivity does not exceed 0.25–0.3, which is due to the low efficiency of the FRET. On the contrary, in a system of reversed micelles, it is difficult to monitor the enzymatic reaction by MUTMAC/MUmb at 450 nm due to the quenching of the product signal; therefore, the sensitivity index for the FRET marker is about 2–3 units. The data obtained using the new FRET approach are consistent with the literature [36–38].

When using small micelles with a degree of hydration of 11, the distance between the fluorophores of the FRET pairs approaches the value $R_0 \sim 5.5$ nm (Figure 1e), which determines the high sensitivity of the FRET method (Figure 2c) in a system of reversed micelles with low degrees of hydration.

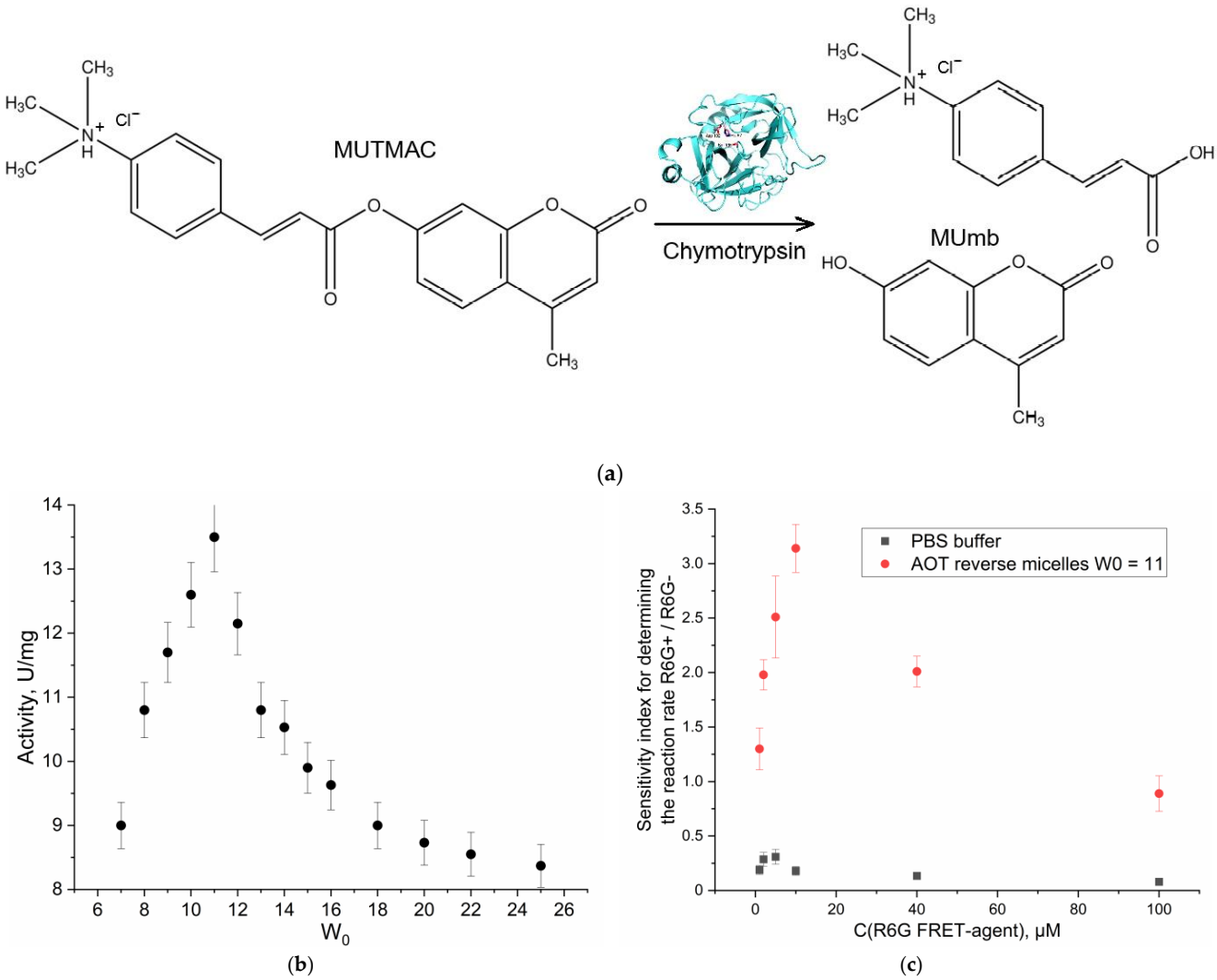

Figure 2. (**a**) The scheme of the catalytic hydrolysis reaction of MUTMAC using α-chymotrypsin. (**b**) The profile of the catalytic activity of chymotrypsin in the system of reversed AOT-octane micelles, depending on the hydration degree W_0. PBS (0.01 M, pH 7.4) was used as aqueous phase. T = 37 °C. (**c**) Kinetic parameters of MUTMAC (0.2 mM) hydrolysis in the presence of chymotrypsin (6 μM) with FRET-marker R6G (variable concentration): sensitivity index for determining the rate of the MUTMAC hydrolysis reaction in the presence of FRET-agent R6G vs. in the absence of R6G. For R6G+ system: λ_{exci} = 360 nm, λ_{emi} = 550 nm; for MUTMAC in R6G absence system: λ_{exci} = 360 nm, λ_{emi} = 450 nm. AOT/octane reverse micelles, W_0 = 11. T = 37 °C.

3.2.4. Acid Phosphatase Activity in Buffer Solution and in AOT-Octane Reverse Micelles

It is interesting to explore this phenomenon of the enhancement of the FRET effect in the reversed micelles system for a membranotropic enzyme that functions in interaction with a micellar matrix compared with aqueous solution. Therefore, we chose acid phosphatase (membrane enzyme, hydrolase) as a model enzyme, which also (as α-chymotrypsin) releases the product MUmb during the enzymatic reaction, forming a donor–acceptor pair with R6G.

The dependence of the maximum rate of hydrolysis of 4-methylumbelliferyl phosphate (MUmb-phosphate) catalyzed by acid phosphatase in the system of reversed AOT cells on the degree of hydration of surfactants is a profile with two optima of enzyme activity at hydration degrees W_0 = 20 and 23–25 (Figure 3a). According to the principle of geometric correspondence, the optima of catalytic activity correspond to the coincidence of the size of the protein of the inner cavity of the micelle. Sedimentation analysis of the micellar system

showed that at a hydration degree of 20, the enzyme functions as a monomer (48 kDa), and at W_0 = 24 as a dimer (98 kDa). At W_0 = 40, acid phosphatase can form tetramers and complexes with large organic molecules [24].

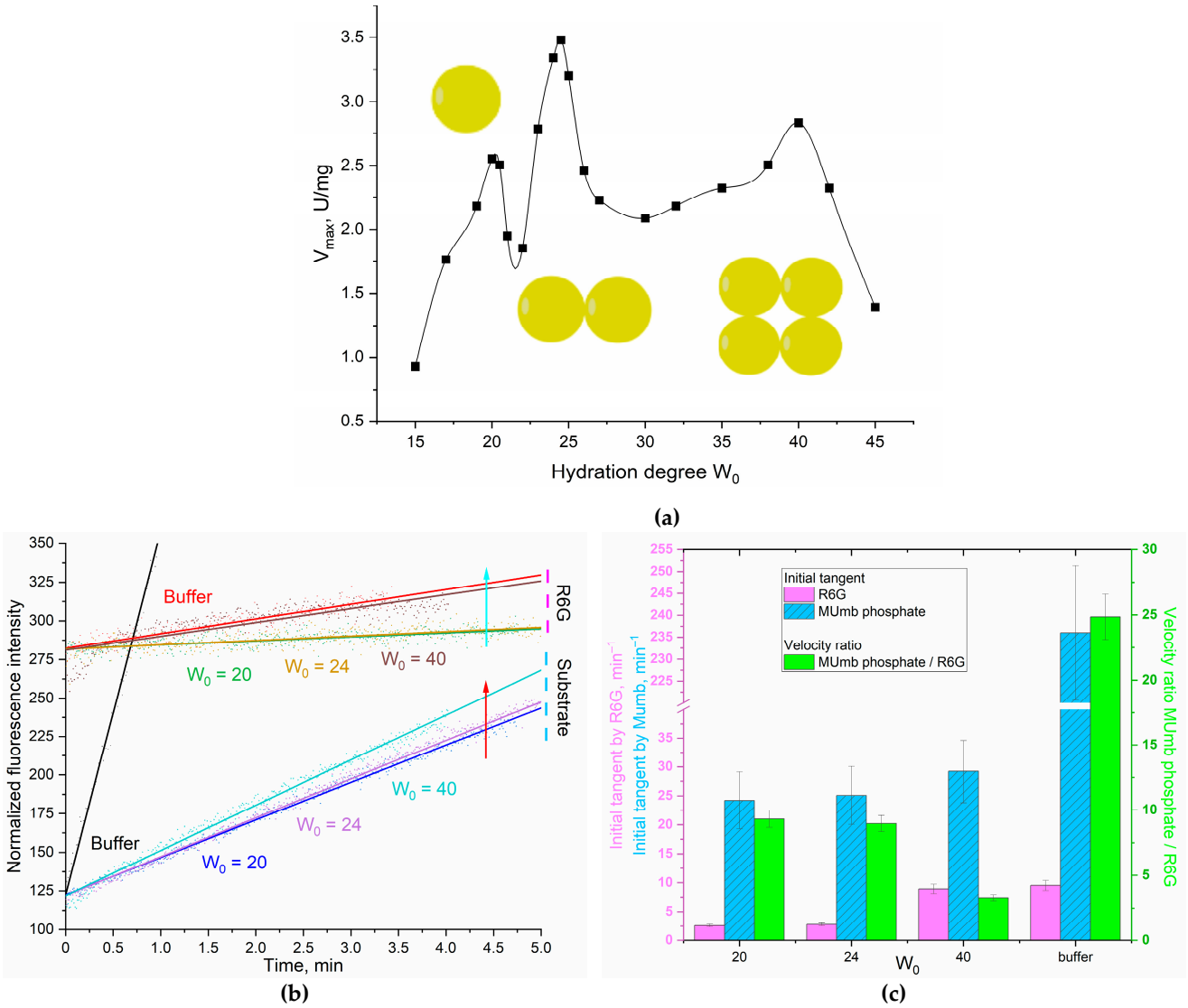

Figure 3. (**a**) The dependence of the catalytic activity (V_{max}) of acid phosphatase on the hydration degree of AOT (W_0) in the reverse micellar system. Note that 0.1M AOT in octane was used as organic phase; KOAc/HOAc (0.01M, pH 4.9) was used as aqueous phase. T = 37 °C. (**b**) Phosphatase activity profiles curves of acid phosphatase (6 μM) in relation to MUmb-phosphate (0.8 mM) with FRET agent R6G-acceptor (2 μM). λ_{exci} = 360 nm, λ_{emi} = 450 (substrate—MUmb-phosphate; product—MUmb), 550 (R6G) nm. AOT/octane reverse micelles. W_0 = 20, 24, 40. KOAc/HOAc (0.01M, pH 4.9) was used as aqueous phase. T = 37 °C. The red and blue ascending arrows indicate an increase in the degree of hydration of the micelles and the transition to a buffer solution. (**c**) Tangents of the initial linear sections of phosphatase profiles, the ratio of the initial "velocities" of the observed signals for the product and for the FRET agent R6G.

Figure 3 shows the profiles of phosphatase activity of acid phosphatase in the acetate buffer and in reversed micelles with hydration degrees W_0 = 20, 24, and 40. Detection was carried out by increasing the fluorescence of the initial reaction product (MUmb-phosphate -> MUmb) and by using the FRET acceptor agent R6G.

Again, in an aqueous solution, there is no special need for R6G: the reaction rate dI/dt = 240 (Figure 3b,c), and only marginal energy is transmitted to R6G, that is, about 4%

(Figure 3c). However, in reversed micelles (W_0 = 40), the product signal (MUmb at 450 nm) is quenched, while on the contrary, R6G fluoresces more intensively. With a decrease in the hydration degree (micellar size), the fluorescence of MUmb decreases by 15–50% due to quenching, but the FRET effect is still pronounced.

The observed rate of the enzymatic reaction tracked by R6G depends on the size of the reversed micelles. At W_0 = 20 or 24, about 10% of the fluorescence signal (velocity dI/dt) passes to R6G, and at W_0 = 40, about 13% of the velocity is transferred to rhodamine. This is due to the optimal size of the inner aqueous phase in the micelles in terms of the FRET condition, including places for the enzyme, substrate, and R6G. Thus, the observed dependence of the energy transfer efficiency to R6G on the product has a minimum at W_0 38–42. With high hydration degrees, we are gradually getting closer to the situation in an aqueous solution. At low degrees of hydration, the micelles have too small an internal cavity to accommodate the optimal amount of substrate and FRET agent (R6G). The catalytic parameters obtained using the new FRET approach are consistent with the literature data obtained by other methods [24,27].

It is worth noting that the FRET agent is used in a deficit (100–500 fold) to obtain comparable fluorescence values. It is possible to increase the amount of R6G, thereby significantly increasing the analytical signal and reducing the required amounts of substrate and enzyme. With an increase in the concentration of R6G by 5 and 20 times, the sensitivity of tracking product accumulation by the FRET marker rhodamine 6G increases by 2.5 and 6 times, respectively. In addition, the shift to the long-wavelength region increases the selectivity of the signal.

There is a significant disparity in the behavior of aqueous and membranotropic enzymes, as exemplified by chymotrypsin when compared with acid phosphatase, with regard to the use of FRET detection. The FRET agent enhances the sensitivity of detecting the reaction rate more effectively in the case of membrane enzymes due to the fact that the enzyme is more densely surrounded by surfactant molecules and embedded within the membrane. Since enzymes containing carbohydrate or lipid groups have membrane-active properties, enzymes of the acid phosphatase are glycosylated. This results in their interaction with the micellar matrix and their high sensitivity to R6G.

3.2.5. Catalytic Activity in a Two-Enzyme System: Alkaline Phosphatase and Asparaginase

Acid phosphatase functions at slightly acidic pH values (about 5–6), but it is important to study the FRET effect also in neutral to weakly alkaline pH (as in the bloodstream). To do this, we used alkaline phosphatase and asparaginase with a pH optimum of about 8.0. Further FRET probes were applied to study the catalytic activity in a two-enzyme system.

Indeed, in research practice in biochemistry, there is often a need to study enzymatic reactions in two-enzyme systems: to increase the sensitivity of the signal, to study the mutual influence in the composition of enzymatic complexes, to study successive enzymatic reactions, to investigate biochemical chains in which the product of one enzyme is a substrate for another (bioconveyer) or the effect of inhibition in cells' biochemistry, and so on. We suggest studying such reactions using the FRET approach developed here. This may be both the parallel accumulation of one fluorophore donor or the accumulation of two consecutive fluorescence donors.

We chose L-asparaginase and alkaline phosphatase as our model enzymes pair. For example, it would be useful to follow the asparaginase activity by R6G when analyzing the activity of asparaginase in the blood serum samples of patients in the treatment of leukemia. L-Asparaginase hydrolyzes the fluorescent substrate Asp-AMC to L-aspartate and AMC, and alkaline phosphatase hydrolyzes MUmb-phosphate to MUmb (Figure 4). The activity of the enzymes was studied in two enzyme systems with a hydration degree W_0 = 40, since both enzymes are active at such a W_0, and can be located in one micelle.

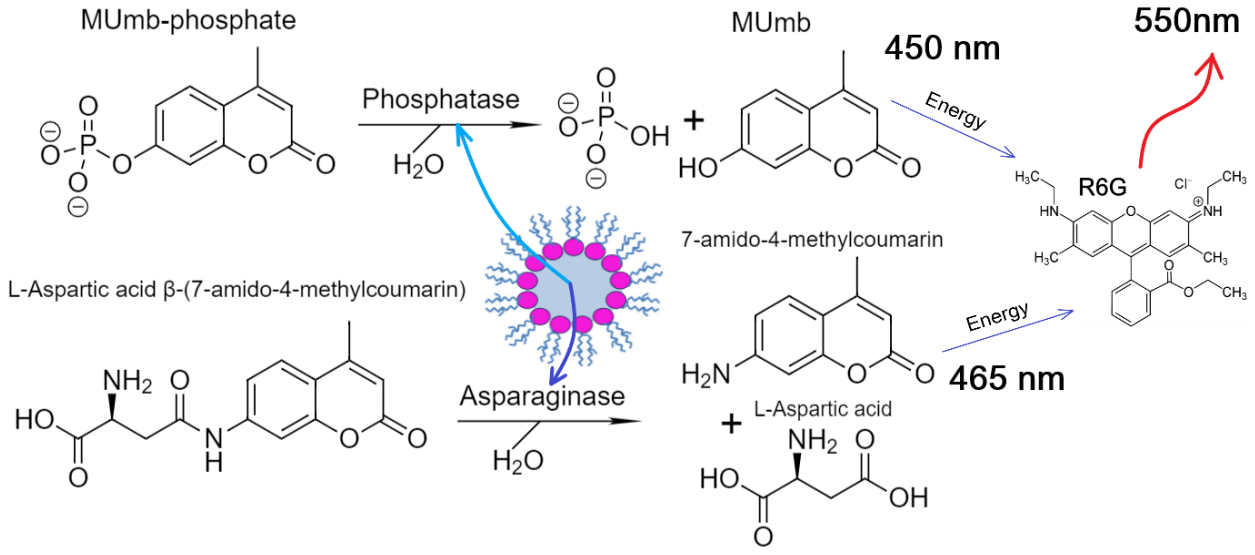

(**a**)

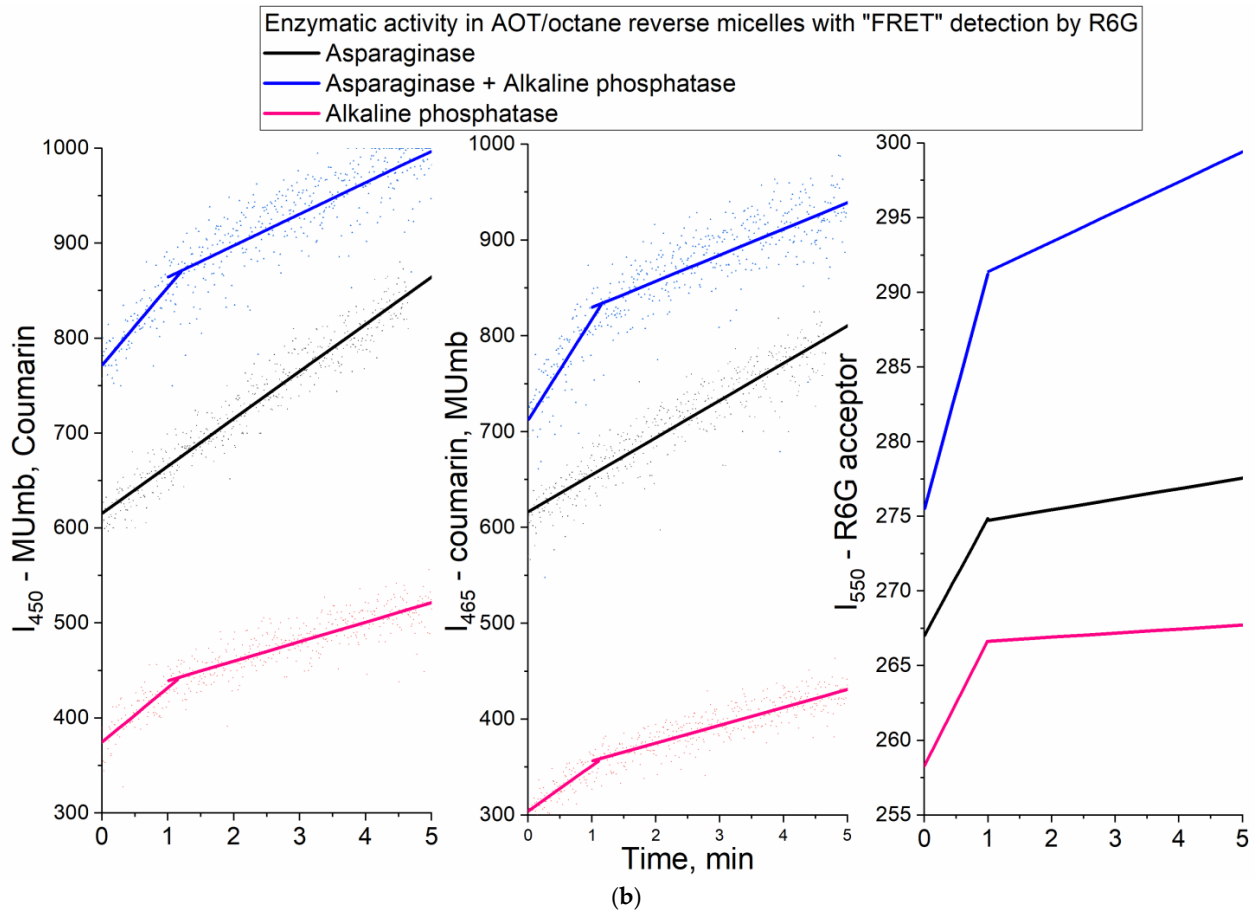

(**b**)

Figure 4. (**a**) Experiment design: Catalytic activity in a two-enzyme system: alkaline phosphatase and asparaginase. (**b**) Activity profile curves of alkaline phosphatase (6 μM) and asparaginase (1 μM) in relation to MUmb-phosphate (0.2 mM) and Asp-AMC (0.2 mM), correspondingly, with FRET agent R6G-acceptor (2 μM). λ_{exci} = 360 nm, λ_{emi} = 450 nm (product 1—MUmb), 465 (product 2—coumarin derivative), 550 nm (R6G—FRET agent). AOT/octane reverse micelles, W_0 = 40. PBS buffer (0.02M, pH 8.2). T = 37 °C.

When using large micelles with a hydration degree of 40, the distance between the fluorophores of the FRET pair approaches the value in an aqueous buffer solution (Figure 1e), which reduces the sensitivity.

Figure 4 shows the kinetic curves of the enzymatic activity of asparaginase, alkaline phosphatase, and their mixed system. The initial linear sections are identified, from which the initial reaction rate can be determined (dI/dt), by initial products as well as by R6G fluorescence increase. Table 1 shows the parameter dI/dt of the initial linear region of kinetic curves.

Table 1. Initial rates of asparaginase and phosphatase kinetic profiles normalized for the concentration of fluorophore. AOT/octane reverse micellar system, W_0 = 40. The conditions are the same as indicated in the caption of Figure 4.

Enzyme/Emission Wavelength	Initial Rate, $mM^{-1} \times min^{-1}$ (the Observed Values of Tangents of Linear Sections of Kinetic Curves)			Specific Activity, U/mg	Fluorescence Quantum Yield φ
	450 nm (AMC > MUmb)	465 nm (MUmb > AMC)	550 nm (R6G)		
L-Asparaginase	245 ± 5	215 ± 5	4000 ± 150	20 ± 3	AMC: 0.12 R6G: 0.75
Alkaline phosphatase	285 ± 20	240 ± 25	4200 ± 250	2.1 ± 0.6	MUmb:0.09 R6G: 0.74
Asparaginase + alkaline phosphatase	410 ± 30	525 ± 35	8000 ± 500	17 ± 4; 2.5 ± 0.8	AMC: 0.13 MUmb: 0.08 R6G: 0.72

In the case of L-asparaginase, approximately 20% of the (dI/dt) product passes to R6G. For alkaline phosphatase, this FRET characteristic is about 15%. In a two-enzyme system, the efficiency of FRET is in the range of 15–20%. Thus, we were able to monitor the enzymatic reactions of hydrolysis using R6G. In general, the obtained data are promising for practical applications in enzymological studies and visualization of processes in the cell using confocal microscopy to reduce autofluorescence.

Thus, using the examples of the four enzymes, we have shown that it is possible to study catalysis using a FRET probe (R6G-acceptor), which makes it possible to significantly increase the anatomical signal and enhance its selectivity by shifting to the red region. In addition, the proposed methods are promising for use as visualizers of cellular structures and on-line reactions.

3.3. Visualization of Enzyme Activity in Living HEK293T Cells

In medical practice, a variety of enzyme preparations are used, including asparaginase for the treatment of leukemia [39–45]. Therefore, targeted delivery of protein molecules to specific cells is a crucial task. The FRET technique allows us to study the intracellular activity of enzymes and determine the effectiveness of drug formulations.

Figure 5 shows confocal images of HEK293T cells, which were pre-incubated with enzyme for different times: in 1 h, the enzyme practically did not accumulate in the cells, while in 4 h, the accumulation of the enzyme was recorded. After that, the cells were placed in an agarose gel with a MUTMAC substrate, and during the enzymatic reaction, a fluorescent product MUmb accumulated. FRET is observed between the substrate or the product with FRET-agent R6G, which makes it possible to determine the accumulation of the latter due to enzymatic activity associated with cells.

These are confocal fluorescence images of HEK293T cells (with pre-absorbed L-asparaginases) in agarose gel containing substrate (initial fluorophore ($\lambda_{exci,max}$ = 360 nm, $\lambda_{emi\ max}$ = 460 nm) − 1 mg/mL MUTMAC and 1 μM FRET-agent R6G ($\lambda_{exci,max}$ = 515 nm, $\lambda_{emi,max}$ = 550 nm)), so in any case, fluorescence from the background is observed due to the presence of a substrate—a background fluorophore in the system. This demonstrates that the system functions effectively and the substrate is uniformly distributed throughout

the gel volume. If the enzyme does not enter the cells, there are no areas of increased fluorescence corresponding to enzyme activity within the cells.

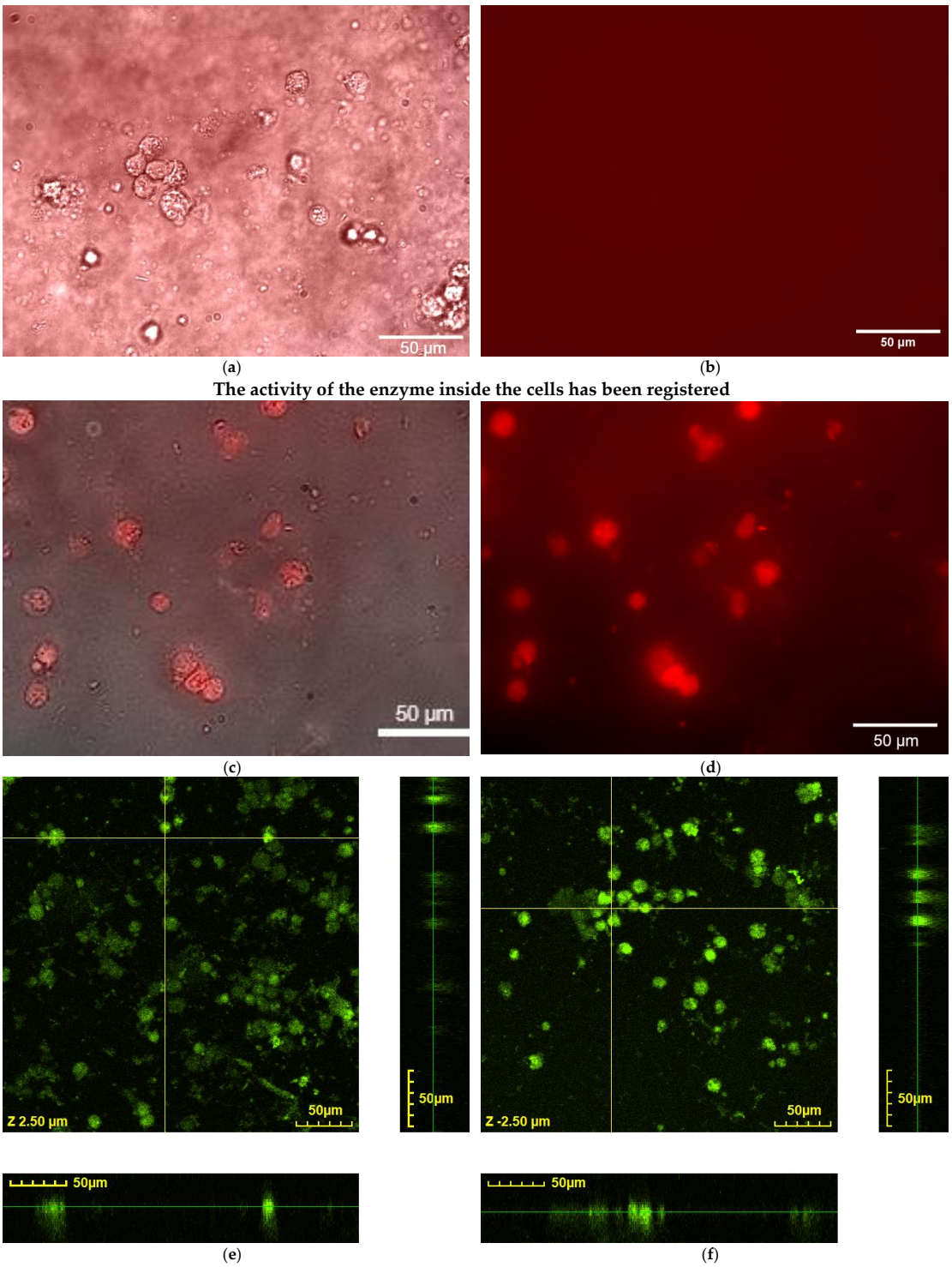

Figure 5. Fluorescence images of HEK293T cells (with absorbed L-asparaginases) in agarose gel containing 1 mg/mL MUTMAC and 1 µM FRET-agent R6G. T = 37 °C. C_0(enzyme) = 0.5 mg/mL. $\lambda_{exci,\ max}$ = 360 nm, λ_{emi} = 425–720 nm. The scale bar is 50 µm. (**a**,**b**) Images of cells after 1 h incubation with the enzyme: merged and R6G fluorescent channel; (**c**,**d**) images of cells after 4 h incubation with the enzyme: merged and R6G fluorescent channel. (**e**,**f**) Confocal fluorescent images of HEK293T cells (with absorbed L-asparaginases) and 3D projections of the cell volume distribution of eosin-labeled asparaginase incubated with cells for 1 and 4 h, respectively. $\lambda_{exci,max}$ = 515 nm, λ_{emi} = 530–580 nm.

With regard to the target signal, specifically the enzyme activity inside cells, we refer to the excessive fluorescence of cells compared to the background, which is due to the fluorescence resonance energy transfer (FRET) phenomenon. This occurs as a result of the release of a fluorescent product ($\lambda_{exci,max}$ = 360 nm, $\lambda_{emi,max}$ = 480 nm) within the cell. This FRET effect can be clearly observed by comparing Figure 5a and Figure 5c. The cell-to-background ratio of fluorescence can be used as a measure of enzyme activity.

Figure 5e,f show the confocal fluorescent images of HEK293T cells (with absorbed L-asparaginases) and 3D projections of the cell volume distribution of eosin-labeled asparaginase incubated with cells for 1 and 4 h, respectively ($\lambda_{exci,max}$ = 515 nm, λ_{emi} = 530–580 nm). These images confirm the penetration of the enzyme into the cells, and not just adsorption on the surface, while the degree of penetration into the cells increases with increasing incubation time from 1 to 4 h.

It has been found that the FRET technique allows us to see firsthand the areas of depletion by the substrate (donor) and enrichment by the product, exactly at the sites of cell localization—in the case of intracellular activity. We also observe an even fluorescent background in the case of asparaginase, which did not internalize into cancer cells. This demonstrates the usefulness of the FRET method for determining enzymatic activity and studying the effectiveness of drugs.

4. Conclusions

In this paper, we propose the use of the fluorescence resonance energy transfer (FRET) probe technique, specifically using rhodamine 6G (R6G), 4-methylumbelliferone (MUmb), and 7-amino-4-methylcoumarin (AMC) derivatives, as a tool for studying enzymatic activity. The proposed method allows one to study enzymatic activity without relying on product detection, and instead using the FRET signal as a marker. This approach has the potential to increase the efficiency and specificity of the assay, as well as the possibility of translating the technique to living cells. Four model enzymes were investigated: acidic and alkaline phosphatase, asparaginase, and chymotrypsin, in aqueous media and reverse AOT-octane micelle systems. In these systems, it was challenging to directly determine the parameters of enzymatic catalysis from the AMC or MUmb product signal. However, by using the R6G FRET marker, we were able to improve the sensitivity of the technique up to 10-fold. We found that the FRET efficiency varied between 5 and 20%, depending on the system composition and enzyme type. The intracellular activity of asparaginase and the non-specific activity of the enzyme observed using the FRET technique can be seen as two opposing aspects of the function of medical enzymes—which is important for determining the specificity of the formulation. The data obtained are promising in terms of studying enzymatic activity in reverse micelle systems as well as living cells.

Author Contributions: Conceptualization, E.V.K. and I.D.Z.; methodology, I.D.Z., A.A.E., E.V.K.; formal analysis, I.D.Z. and A.A.E.; investigation, I.D.Z., A.A.E. and E.V.K.; data curation, I.D.Z. and A.A.E.; writing—original draft preparation, I.D.Z.; writing—review and editing, E.V.K.; project supervision, E.V.K.; funding acquisition, E.V.K. All authors have read and agreed to the published version of the manuscript.

Funding: This research was funded by the Russian Science Foundation, grant number 24-25-00104.

Institutional Review Board Statement: HEK293T cell line was obtained from Lomonosov Moscow State University Depository of Live Systems Collection (Moscow, Russia).

Informed Consent Statement: Not applicable.

Data Availability Statement: The data presented in this study are available in the main text.

Acknowledgments: This work was performed using the following equipment from the program for the development of Moscow State University: FTIR microscope MICRAN-3, Jasco J-815 CD Spectrometer, and AFM microscope NTEGRA II.

Conflicts of Interest: The authors declare no conflicts of interest.

Abbreviations

AMC—7-amino-4-methylcoumarin; AOT—bis(2-ethylhexyl) sulfosuccinate or diisooctyl sulfosuccinate; FRET—Förster resonance energy transfer; MUmb—4-methylumbelliferone or methylumbelliferyl; MUTMAC—4-methylumbelliferyl p-trimethylammoniocinnamate chloride; R6G—rhodamine 6G; W_0—degree of hydration of reversed micelles.

References

1. Krasteva, G.; Pfeil, U.; Drab, M.; Kummer, W.; König, P. Caveolin-1 and -2 in Airway Epithelium: Expression and in Situ Association as Detected by FRET-CLSM. *Respir. Res.* **2006**, *7*, 1–13. [CrossRef] [PubMed]
2. Yang, Y.; Liu, H.; Han, M.; Sun, B.; Li, J. Multilayer Microcapsules for FRET Analysis and Two-Photon-Activated Photodynamic Therapy. *Angew. Chemie Int. Ed.* **2016**, *55*, 13538–13543. [CrossRef] [PubMed]
3. König, P.; Krasteva, G.; Tag, C.; König, I.R.; Arens, C.; Kummer, W. FRET-CLSM and Double-Labeling Indirect Immunofluorescence to Detect Close Association of Proteins in Tissue Sections. *Lab. Investig.* **2006**, *86*, 853–864. [CrossRef] [PubMed]
4. Chen, T.; He, B.; Tao, J.; He, Y.; Deng, H.; Wang, X.; Zheng, Y. Application of Förster Resonance Energy Transfer (FRET) Technique to Elucidate Intracellular and In Vivo Biofate of Nanomedicines. *Adv. Drug Deliv. Rev.* **2019**, *143*, 177–205. [CrossRef] [PubMed]
5. Fuenzalida, J.P.; Weikert, T.; Hoffmann, S.; Vila-Sanjurjo, C.; Moerschbacher, B.M.; Goycoolea, F.M.; Kolkenbrock, S. Affinity Protein-Based FRET Tools for Cellular Tracking of Chitosan Nanoparticles and Determination of the Polymer Degree of Acetylation. *Biomacromolecules* **2014**, *15*, 2532–2539. [CrossRef] [PubMed]
6. Kaminski Schierle, G.S.; Bertoncini, C.W.; Chan, F.T.S.; van der Goot, A.T.; Schwedler, S.; Skepper, J.; Schlachter, S.; van Ham, T.; Esposito, A.; Kumita, J.R.; et al. A FRET Sensor for Non-Invasive Imaging of Amyloid Formation in Vivo. *ChemPhysChem* **2011**, *12*, 673–680. [CrossRef] [PubMed]
7. Jares-Erijman, E.A.; Jovin, T.M. FRET Imaging. *Nat. Biotechnol.* **2003**, *21*, 1387–1395. [CrossRef] [PubMed]
8. Huang, P.; Song, H.; Zhang, Y.; Liu, J.; Cheng, Z.; Liang, X.J.; Wang, W.; Kong, D.; Liu, J. FRET-Enabled Monitoring of the Thermosensitive Nanoscale Assembly of Polymeric Micelles into Macroscale Hydrogel and Sequential Cognate Micelles Release. *Biomaterials* **2017**, *145*, 81–91. [CrossRef] [PubMed]
9. Meng, F.; Sachs, F. Orientation-Based FRET Sensor for Real-Time Imaging of Cellular Forces. *J. Cell Sci.* **2012**, *125*, 743–750. [CrossRef]
10. Kikuchi, K.; Takakusa, H.; Nagano, T. Recent Advances in the Design of Small Molecule-Based FRET Sensors for Cell Biology. *TrAC—Trends Anal. Chem.* **2004**, *23*, 407–415. [CrossRef]
11. Lindenburg, L.; Merkx, M. Engineering Genetically Encoded FRET Sensors. *Sensors* **2014**, *14*, 11691–11713. [CrossRef] [PubMed]
12. Dennis, A.M.; Rhee, W.J.; Sotto, D.; Dublin, S.N.; Bao, G. Quantum Dot-Fluorescent Protein Fret Probes for Sensing Intracellular PH. *ACS Nano* **2012**, *6*, 2917–2924. [CrossRef] [PubMed]
13. Panniello, A.; Trapani, M.; Cordaro, M.; Dibenedetto, C.N.; Tommasi, R.; Ingrosso, C.; Fanizza, E.; Grisorio, R.; Collini, E.; Agostiano, A.; et al. High-Efficiency FRET Processes in BODIPY-Functionalized Quantum Dot Architectures. *Chem.—A Eur. J.* **2021**, *27*, 2371–2380. [CrossRef] [PubMed]
14. De Los Santos, C.; Chang, C.; Mycek, M.; Cardullo, R.A. FRAP, FLIM, and FRET: Detection and Analysis of Cellular Dynamics on a Molecular Scale Using Fluorescence Microscopy. *Mol. Reprod. Dev.* **2015**, *82*, 587–604. [CrossRef] [PubMed]
15. Provenzano, P.P.; Eliceiri, K.W.; Keely, P.J. Multiphoton Microscopy and Fluorescence Lifetime Imaging Microscopy (FLIM) to Monitor Metastasis and the Tumor Microenvironment. *Clin. Exp. Metastasis* **2009**, *26*, 357–370. [CrossRef] [PubMed]
16. Ma, Y.; Lee, Y.; Best-Popescu, C.; Gao, L. High-Speed Compressed-Sensing Fluorescence Lifetime Imaging Microscopy of Live Cells. *Proc. Natl. Acad. Sci. USA* **2021**, *118*. [CrossRef] [PubMed]
17. Blacker, T.S.; Mann, Z.F.; Gale, J.E.; Ziegler, M.; Bain, A.J.; Szabadkai, G.; Duchen, M.R. Separating NADH and NADPH Fluorescence in Live Cells and Tissues Using FLIM. *Nat. Commun.* **2014**, *5*. [CrossRef] [PubMed]
18. Eichorst, J.P.; Clegg, R.M.; Wang, Y. Red-Shifted Fluorescent Proteins Monitor Enzymatic Activity in Live HT-1080 Cells with Fluorescence Lifetime Imaging Microscopy (FLIM). *J. Microsc.* **2012**, *248*, 77–89. [CrossRef] [PubMed]
19. Shrestha, D.; Jenei, A.; Nagy, P.; Vereb, G.; Szöllősi, J. Understanding FRET as a Research Tool for Cellular Studies. *Int. J. Mol. Sci.* **2015**, *16*, 6718–6756. [CrossRef]
20. Lundin, M.; Blomberg, E.; Tilton, R.D. Polymer Dynamics in Layer-by-Layer Assemblies of Chitosan and Heparin. *Langmuir* **2010**, *26*, 3242–3251. [CrossRef] [PubMed]
21. Abel, S.; Sterpone, F.; Bandyopadhyay, S.; Marchi, M. Molecular Modeling and Simulations of AOT-Water Reverse Micelles in Isooctane: Structural and Dynamic Properties. *J. Phys. Chem. B* **2004**, *108*, 19458–19466. [CrossRef]
22. Abel, S.; Waks, M.; Marchi, M. Molecular Dynamics Simulations of Cytochrome c Unfolding in AOT Reverse Micelles: The First Steps. *Eur. Phys. J. E* **2010**, *32*, 399–409. [CrossRef] [PubMed]
23. Van Horn, W.D.; Ogilvie, M.E.; Flynn, P.F. Use of Reverse Micelles in Membrane Protein Structural Biology. *J. Biomol. NMR* **2008**, *40*, 203–211. [CrossRef] [PubMed]

24. Kudryashova, E.V.; Bronza, V.L.; Vinogradov, A.A.; Kamyshny, A.; Magdassi, S.; Levashov, A.V. Regulation of Acid Phosphatase in Reverse Micellar System by Lipids Additives: Structural Aspects. *J. Colloid Interface Sci.* **2011**, *353*, 490–497. [CrossRef] [PubMed]
25. Creagh, A.L.; Prausnitz, J.M.; Blanch, H.W. Structural and Catalytic Properties of Enzymes in Reverse Micelles. *Enzyme Microb. Technol.* **1993**, *15*, 383–392. [CrossRef] [PubMed]
26. Lin, C.; Zhao, J.; Jiang, R. Nile Red Probing for the Micelle-to-Vesicle Transition of AOT in Aqueous Solution. *Chem. Phys. Lett.* **2008**, *464*, 77–81. [CrossRef]
27. Luchter-Wasylewska, E.; Iciek, M. Positive Cooperativity in Substrate Binding of Human Prostatic Acid Phosphatase Entrapped in AOT-Isooctane-Water Reverse Micelles. *J. Colloid Interface Sci.* **2004**, *273*, 632–637. [CrossRef] [PubMed]
28. Sahu, K.; Ghosh, S.; Mondal, S.K.; Ghosh, B.C.; Sen, P.; Roy, D.; Bhattacharyya, K. Ultrafast Fluorescence Resonance Energy Transfer in a Micelle. *J. Chem. Phys.* **2006**, *125*, 1–9. [CrossRef]
29. Ilhami, F.B.; Bayle, E.A.; Cheng, C.C. Complementary Nucleobase Interactions Drive Co-Assembly of Drugs and Nanocarriers for Selective Cancer Chemotherapy. *Pharmaceutics* **2021**, *13*, 1–18. [CrossRef] [PubMed]
30. Ngan, V.T.T.; Chiou, P.Y.; Ilhami, F.B.; Bayle, E.A.; Shieh, Y.T.; Chuang, W.T.; Chen, J.K.; Lai, J.Y.; Cheng, C.C. A CO_2-Responsive Imidazole-Functionalized Fluorescent Material Mediates Cancer Chemotherapy. *Pharmaceutics* **2023**, *15*, 354. [CrossRef]
31. Zehentbauer, F.M.; Moretto, C.; Stephen, R.; Thevar, T.; Gilchrist, J.R.; Pokrajac, D.; Richard, K.L.; Kiefer, J. Fluorescence Spectroscopy of Rhodamine 6G: Concentration and Solvent Effects. *Spectrochim. Acta—Part A Mol. Biomol. Spectrosc.* **2014**, *121*, 147–151. [CrossRef]
32. Zlotnikov, I.D.; Malashkeevich, S.M.; Belogurova, N.G.; Kudryashova, E.V. Thermoreversible Gels Based on Chitosan Copolymers as "Intelligent" Drug Delivery System with Prolonged Action for Intramuscular Injection. *Pharmaceutics* **2023**, *15*, 1478. [CrossRef] [PubMed]
33. Zlotnikov, I.D.; Savchenko, I.V.; Kudryashova, E. V Specific FRET Probes Sensitive to Chitosan-Based Polymeric Micelles Formation, Drug-Loading, and Fine Structural Features. *Polymers* **2024**, *16*, 739. [CrossRef] [PubMed]
34. Kudryashova, E.V.; Leferink, N.G.H.; Slot, I.G.M.; Van Berkel, W.J.H. Galactonolactone Oxidoreductase from Trypanosoma Cruzi Employs a FAD Cofactor for the Synthesis of Vitamin C. *Biochim. Biophys. Acta—Proteins Proteomics* **2011**, *1814*, 545–552. [CrossRef] [PubMed]
35. Maitra, A.; Ghosh, P.K.; De, T.K.; Sahoo, S.K. Process for the Preparation of Highly Monodispersed Polymeric Hydrophilic Nanoparticles. U.S. Patent 5874111A, 7 January 1997.
36. Jia, H.; Zhu, G.; Wang, P. Catalytic Behaviors of Enzymes Attached to Nanoparticles: The Effect of Particle Mobility. *Biotechnol. Bioeng.* **2003**, *84*, 406–414. [CrossRef] [PubMed]
37. Blocher, M.; Walde, P.; Dunn, I.J. Modeling of Enzymatic Reactions in Vesicles: The Case of Chymotrypsin. *Biotechnol. Bioeng.* **1999**, *62*, 36–43. [CrossRef]
38. Kudryashova, E.V.; Artemova, T.M.; Vinogradov, A.A.; Gladilin, A.K.; Mozhaev, V.V.; Levashov, A.V. Stabilization and Activation of α-Chymotrypsin in Water-Organic Solvent Systems by Complex Formation with Oligoamines. *Protein Eng.* **2003**, *16*, 303–309. [CrossRef] [PubMed]
39. Batool, T.; Makky, E.A.; Jalal, M.; Yusoff, M.M. A Comprehensive Review on L-Asparaginase and Its Applications. *Appl. Biochem. Biotechnol.* **2016**, *178*, 900–923. [CrossRef] [PubMed]
40. Fonseca, M.H.G.; da Silva Fiúza, T.; de Morais, S.B.; Trevizani, R. Circumventing the Side Effects of L-Asparaginase. *Biomed. Pharmacother.* **2021**, *139*, 111616. [CrossRef] [PubMed]
41. Burke, M.J.; Zalewska-Szewczyk, B. Hypersensitivity Reactions to Asparaginase Therapy in Acute Lymphoblastic Leukemia: Immunology and Clinical Consequences. *Futur. Oncol.* **2022**, *18*, 1285–1299. [CrossRef]
42. Egler, R.A.; Ahuja, S.P.; Matloub, Y. L-Asparaginase in the Treatment of Patients with Acute Lymphoblastic Leukemia. *J. Pharmacol. Pharmacother.* **2016**, *7*, 62–71. [CrossRef]
43. Krasotkina, J.; Borisova, A.A.; Gervaziev, Y.V.; Sokolov, N.N. One-Step Purification and Kinetic Properties of the Recombinant L-Asparaginase from Erwinia Carotovora. *Biotech. Appl. Biochem.* **2004**, *39*, 215–221. [CrossRef] [PubMed]
44. Douer, D.; Gökbuget, N.; Stock, W.; Boissel, N. Optimizing Use of L-Asparaginase–Based Treatment of Adults with Acute Lymphoblastic Leukemia. *Blood Rev.* **2022**, *53*. [CrossRef] [PubMed]
45. Mohideen, A.K.S. Molecular Docking Study of L-Asparaginase i from Vibrio Campbellii in the Treatment of Acute Lymphoblastic Leukemia (ALL). *EuroBiotech J.* **2020**, *4*, 8–16. [CrossRef]